CO/CO_2 Potentiometric Titrations of Carbon Monoxide Dehydrogenase from *Clostridium thermoaceticum* and the Effect of CO_2[†]

William K. Russell and Paul A. Lindahl*

Department of Chemistry, Texas A&M University, College Station, Texas 77843

Received January 21, 1998; Revised Manuscript Received April 22, 1998

ABSTRACT: Acetogenic carbon monoxide dehydrogenases catalyze the reversible oxidation of CO to CO_2 and the synthesis of acetyl-coenzyme A, utilizing two novel Ni-Fe-S active sites (the C- and A-clusters, respectively) and an $[Fe_4S_4]^{2+/1+}$ cluster (the B-cluster) that serves to transfer electrons. Enzyme samples were titrated under equilibrium conditions using various partial pressures of CO in Ar and CO_2 atmospheres. EPR signal intensities from each cluster were analyzed as a function of potential using the Nernst equation. The presence of CO_2 raised the reduction potentials of the A-, B-, and C-clusters, and it appeared to increase the strength of CO (substrate for acetyl-CoA synthesis) binding to the reduced A-cluster. Carbon dioxide also appeared to stabilize an intermediate EPR-silent state of the C-cluster and alter the saturation/relaxation properties of the reduced B-cluster. Simulations assuming *n* values (number of e^- involved in reduction) larger than appropriate for the *individual* reactions generally fit better to the titration data than those which assumed the appropriate n, indicating positive redox cooperativity. Carbon dioxide did not inhibit 1,10-phenanthroline from removing the labile Ni from the A-cluster, but it did inhibit the CO/acetyl-coenzyme A exchange activity, probably by causing CO to bind more tightly to the A-cluster. Taken together, these results indicate a significant CO_2-dependent conformational change affecting the properties of all three clusters and both subunits. Since the enzyme operates in vivo in a CO_2 environment, the CO_2-induced conformation may be mechanistically important.

Carbon monoxide dehydrogenases are one of only five known types of Ni-containing enzymes. They are found in certain acetogenic, methanogenic, photosynthetic, and sulfate-reducing bacteria (*1*) and catalyze the reversible oxidation of CO to CO_2 according to eq 1.

$$CO + H_2O \rightleftharpoons CO_2 + 2H^+ + 2e^- \qquad (1)$$

The enzyme from the acetogen *Clostridium thermoaceticum* (CODH)[1] also catalyzes the synthesis of acetyl-coenzyme A from CO, coenzyme A, and a methyl group (*2*). It is an $\alpha_2\beta_2$ tetramer (*3*) containing ∼ 4 Ni, 24 Fe and 30 S^{2-} ions, organized into three clusters called A, B, and C.

The C-cluster is the active site for CO oxidation/CO_2 reduction (*4*). It has a Ni-X-Fe_4S_4 structure (*5*), and is located in the β-subunit (*3*). The diamagnetic oxidized form (C_{ox}) can be reduced by one electron to a state (C_{red1}) that exhibits an EPR signal with $g_{av} = 1.82$ (*6*).

The B-cluster is a typical $[Fe_4S_4]^{2+/1+}$ cluster (*7*) also located in the β-subunit (*3*). It serves as an $n = 1$ electron shuttle between the other clusters in the enzyme and external redox agents (*8*, *9*). The diamagnetic oxidized form (B_{ox}) can be reduced by one electron to a state (B_{red}) yielding a $g_{av} = 1.94$ signal (*6*).

Lindahl et al. (*6*) measured the thermodynamic reduction potentials for the B_{ox}/B_{red} and C_{ox}/C_{red1} couples electrochemically, and obtained $E^0_B(7.2) = -0.44$ V and $E^0_{C1}(7.2) = -0.22$ V. Similar potentials (ranging from −0.39 V to −0.44 V for E^0_B and −0.035 V to −0.23 V for E^0_{C1}) have been obtained for the corresponding redox couples in CODHs isolated from other bacteria (*5*).

At substantially lower potentials, in accordance with $E^m = -0.53$ V, the $g_{av} = 1.82$ signal from C_{red1} disappears and is replaced by another EPR signal with $g_{av} = 1.86$ (*6*), arising from a state designated C_{red2}. C_{red2} is probably two electrons more reduced than C_{red1} (*9*, *10*), but the exact electronic designation is not certain. During catalysis, CO is thought to bind C_{red1}, be attacked by OH^-, deliver two electrons to C_{red1} (affording C_{red2}), and dissociate as CO_2 (*9*, *11*). An electron from C_{red2} is presumed to transfer to B_{ox}, resulting

[†] This research was supported by the National Institutes of Health (GM46441) and the Robert A. Welch Foundation (A1170).

* Author to whom correspondence should be addressed. Email: Lindahl@chemvx.tamu.edu.

[1] Abbreviations: CODH, carbon monoxide dehydrogenase from *Clostridium thermoaceticum*; CoA, coenzyme A; A_{ox}, A_{red}, and A_{red}-CO, oxidized, one-electron-reduced (hypothetical), and one-electron-reduced-and-CO-bound states of the A-cluster, respectively; B_{ox} and B_{red}, oxidized and reduced states of the B-cluster, respectively; C_{ox}, C_{red1}, and C_{red2}, oxidized, one-electron-reduced, and (most likely) three-electron-reduced states of the C-cluster, respectively; C_{int}, hypothetical state of the C-cluster presumed to be one electron more reduced than C_{red1} and one electron more oxidized than C_{red2}; E^0_A, E^0_B(pH), E^0_{C1}(pH), E^0_{C12}(pH), E^0_{C1N}(pH), E^0_{CN2}(pH), and E^0_{CO/CO_2}(pH), the A_{ox}/A_{red}, B_{ox}/B_{red}, C_{ox}/C_{red1}, C_{red1}/C_{red2}, C_{red1}/C_{int}, C_{int}/C_{red2}, and CO/CO_2 half-cell standard reduction potentials, respectively, at an indicated pH (6.3, 7.0, or 8.0); E^0_{NiFeC}, standard reduction potential for the A_{ox}/A_{red}-CO half-cell reaction involving a one-electron reduction and CO binding process; E^m_{NiFeC}, midpoint potential for the NiFeC potentiometric titration curve; K_{CO}, the association constant for the binding of CO to A_{red}; P_{CO} and P_{CO_2}, partial pressure of CO and CO_2, respectively; pCO, negative logarithm of P_{CO}; P_{mw}, microwave power; Q_{fit}, quality-of-fit parameter; Q_{bf}, smallest (best) Q_{fit}.

S0006-2960(98)00149-4 CCC: $15.00
Published on Web 06/20/1998

in B_{red} and an as-yet unestablished even-spin C-cluster state called C_{int} (*10*). C_{int} is thought to reoxidize to C_{red1} as electrons exit the enzyme through the B-cluster. In the reverse direction, C_{red2} binds CO_2 and reduces it to CO which dissociates from C_{red1}.

The A-cluster is a Ni-X-Fe_4S_4 cluster that serves as the site of acetyl-CoA synthesis, and resides in the α-subunit (*3, 12*−*17*). By exposing the enzyme to CO, the diamagnetic oxidized state of the A-cluster (A_{ox}) can be reduced to an $S = {}^1/_2$ CO-bound form (A_{red}-CO) that exhibits the so-called NiFeC EPR signal (*6, 7, 18, 19)*. The A_{red} state without CO bound has not been demonstrated. The A-cluster is reduced by electrons from CO oxidation. The NiFeC signal develops 2000 times more slowly than the C-cluster reduces the B-cluster (*8*, *9*), suggesting that the electron pathway from the C- to the A-cluster differs from that used to exit the enzyme through the B-cluster.

One peculiar property of the A-cluster is that it can be reduced only by a very limited group of reductants, including CO. Low-potential reductants such as dithionite or viologens are effective, but only if CO_2, CS_2, or acetyl-CoA are also included (*6, 9, 10, 15, 20)*. The basis of this unusual property is not understood; CO_2 and CS_2 may bind to the enzyme and permit dithionite and viologens to reduce A_{ox}, either directly, or via another cluster in the enzyme (*9*, *10*, *20*).

A number of studies have attempted to analyze the redox behavior of CODH. Lindahl et al. (*6*) electrochemically poised CODH under a CO_2 atmosphere and monitored the NiFeC signal intensity as a function of potential. They concluded that the midpoint potential associated with the development of the NiFeC signal (E^m_{NiFeC}) is between −0.35 V and −0.53 V. Gorst and Ragsdale (*15*) electrochemically poised CODH in the presence of acetyl-CoA. They monitored the development of the NiFeC signal as a function of potential, and fitted the resulting titration curve to the Nernst equation using $E^m_{NiFeC} = -0.541$ V. Shin and Lindahl (*16*) added CO to dithionite-reduced CODH. They monitored the NiFeC signal intensity versus the number of equivalents of CO added, simulated the resulting NiFeC titration curve, and obtained a CO-binding constant K_{CO} of 6−14 atm^{-1}.[2] Although these studies contribute substantially to our understanding of the redox clusters of CODH, each is flawed in some respect (either by not being at equilibrium when samples were frozen, or by assuming that the NiFeC titration curve reflects a simple one-electron reduction). Additionally, CODH has been studied primarily in an inert atmosphere, even though CO_2 is present when the enzyme functions in vivo (the bacteria grow under CO_2). Thus, the properties of CODH examined in the absence of CO_2 and the mechanistic insights gleaned therefrom may not reflect how the enzyme functions in nature.

In this paper we report the results of a series of redox titrations using increasing partial pressures of CO in the presence and absence of CO_2 and reevaluate the results of the previous studies mentioned above. These titrations demonstrate that CO_2 binding substantially changes the redox and CO binding properties of the clusters and provide evidence for cooperative redox behavior. We also report that CO_2 alters the relaxation/saturation properties of the reduced B-cluster and inhibits the CO/acetyl-CoA exchange reaction. Mechanistic implications of these effects are discussed.

EXPERIMENTAL PROCEDURES

CODH Purification and Activities. CODH was grown, purified, and characterized from *C. thermoaceticum* as previously described (*21*). All experiments involving CODH were performed anaerobically in an Ar atmosphere glovebox (Vacuum/Atmospheres HE-453) maintained at ∼300 K with <1 ppm O_2 (monitored by a Teledyne model 310 analyzer). Five batches were isolated, with purities >90% according to SDS−polyacrylamide gel electrophoresis. Protein concentrations were determined by the Biuret method (*22*), assuming 154 700 Da for each CODH $\alpha\beta$ dimer (*23*). Batches had CO oxidation activities of 280, 320, 340, 290, and 290 units/mg (*21)* and CO/acetyl-CoA exchange activities (*24*) of 0.1, 0.07, 0.14, 0.09, and 0.3 units/mg, respectively. For the CO/acetyl-CoA activity in a CO_2 atmosphere, a sample of CODH (0.4 mg, batch 5) was divided in two, and assayed as above except that the cuvette in which one aliquot was assayed contained 0.2 atm CO and 0.8 atm CO_2, while the control contained 0.2 atm CO and 0.8 atm Ar. Two similar experiments (using 0.3 mg CODH per aliquot) were performed using batch 4. CODH was treated with 10 equiv/$\alpha\beta$ of 1,10-phenanthroline as described (*17*), except that the treatment was performed under 1 atm CO_2.

CO Titrations under an Ar Atmosphere. Rubber septa and volume-calibrated EPR tubes (Wilmad, 710-SQ-250m) and vials (Wheaton, 10, 15, and 50 mL) were stored in the glovebox for at least 3 days prior to use. Septum-sealed, Ar-filled tubes and vials were injected by syringe (10, 25, 50, and 100 μL Hamilton gastight series 1700) with O_2-scrubbed (Oxisorb, MG Scientific) research-grade CO (MG Industries). Gases were mixed by withdrawing and reinjecting a syringe-volume of the tube's atmosphere ∼20 times and waiting 1 h to allow for diffusion-mixing. Samples of CODH batches 1 and 2 were rendered free of dithionite and DTT using gel filtration columns (1 cm × 12 cm) of Sephadex G-25 (Pharmacia) equilibrated in 50 mM Tris-Cl, pH 8.0. Aliquots (400 μL of 3.4 mg/mL of batch 1, or 4.1 mg/mL of batch 2) were injected into the EPR tubes and vials. They were thoroughly exposed to the gas phase by agitation, incubated for 3 h, and agitated again. The samples in vials were transferred into EPR tubes (containing the same atmosphere as the vials), and all tubes were frozen in liquid N_2 for subsequent EPR analysis. A similar experiment was performed using a sample (4.2 mg/mL, batch 4) equilibrated in 50 mM MES, pH 6.3. All potentials quoted are vs the Normal Hydrogen Electrode and have an estimated overall uncertainty of ± 0.03 V, unless mentioned otherwise.

CO Titration under a CO_2 Atmosphere at pH 6.3. The titration was performed as above, except that volume-calibrated vials (10, 15, 20, and 60 mL) were filled with slightly greater than 1 atm of O_2-scrubbed CO_2 (dispensed from a Schlenk line) rather than Ar. Samples of CODH (450 μL of 4.8 mg/mL of batch 2, or 4.6 mg/mL of batch 3, in 50 mM Tris-Cl, pH 8) were injected into the vials, incubated for 3 h, then transferred into CO_2-filled EPR tubes and immediately frozen using liquid-N_2-cooled isopentane. The pH of equivalent samples stabilized at 6.3 upon exposure to CO_2.

[2] They actually reported K_{CO} in units of M^{-1}, (6000−14000 M^{-1}; $K_d = 1/K_{CO} = 70-165$ μM) rather than in atm^{-1}. P_{CO} and concentrations of CO in solution were interconverted using the Henry's Law constant of 1.02×10^{-3} μM/atm (*16, 45, 46*).

Reaction of CODH with Ti(III) Citrate and Acetyl-CoA. A sample of CODH (batch 5) was rendered free of reductants as above. Three modified EPR cuvettes with quartz mixing chips (*16*) were filled completely with the reductant-free CODH (500 μL of 13 mg/mL). A solution of Ti(III) citrate was prepared as described (*25*) and 10 equiv/$\alpha\beta$ were added to each cuvette. After 3 min, 0, 0.1, and 3.0 equiv/$\alpha\beta$ of acetyl-CoA (Sigma) were added to different cuvettes. Solutions were mixed, frozen after 15 min incubation, and analyzed by EPR. Another aliquot of enzyme (the positive control) was treated with 1 atm CO prior to freezing.

EPR Characterization. The spectrometer used has been described previously (*16*). Individual EPR signals (g_{av} = 1.82, 1.86, and 1.94) in a given spectrum were simulated using the XPOW program (*26*−*29*). The intensities of simulated EPR signals were adjusted to match those of the observed signals, and then quantified by double integration (*30*) using 1.00 mM CuEDTA as a standard. NiFeC signals were quantified directly from spectra obtained at 130 K. The spin intensities obtained for the g_{av} = 1.82, 1.86, 1.94, and NiFeC signals in an Ar atm (pH = 8) were normalized by dividing by 0.28, 0.21, 0.77, and 0.18 spin/$\alpha\beta$ respectively (these values were the averaged spin intensities of five data points in the plateau region of each titration curve). Corresponding normalization values were 0.22, 0.21, 0.60, and 0.15 spin/$\alpha\beta$ for the Ar pH 6.3 titration and 0.40, 0.40, 0.69, and 0.21 spin/$\alpha\beta$ for the CO_2 titration. In the CO_2 titration, there was no plateau region for the C_{red1} titration curve, and so the normalization value for that curve was assumed to equal that for the C_{red2} curve. Normalized intensities for the g_{av} = 1.82, 1.86, 1.94, and NiFeC signals were plotted versus the negative log of P_{CO} (pCO) to yield the C_{red1}, C_{red2}, B_{red}, and A_{red}-CO titration curves, respectively.

Titration Curve Simulations. Titration curves were simulated using eqs 2−13.[3]

$$2A_{ox} + 3CO \rightleftharpoons 2A_{red}\text{-}CO + CO_2 \quad (2)$$

$$2A_{ox} + CO \rightleftharpoons 2A_{red} + CO_2 \quad (3)$$

$$A_{ox} + CO \rightleftharpoons A_{red} + CO_2 \quad (4)$$

$$A_{red} + CO \rightleftharpoons A_{red}\text{-}CO \quad (5)$$

$$2B_{ox} + CO \rightleftharpoons 2B_{red} + CO_2 \quad (6)$$

$$B_{ox} + CO \rightleftharpoons B_{red} + CO_2 \quad (7)$$

$$C_{red1} + CO \rightleftharpoons C_{red2} + CO_2 \quad (8)$$

$$2C_{red1} + CO \rightleftharpoons 2C_{int} + CO_2 \quad (9)$$

$$2C_{int} + CO \rightleftharpoons 2C_{red2} + CO_2 \quad (10)$$

$$C_{red1} + 2CO \rightleftharpoons C_{red2} + 2CO_2 \quad (11)$$

$$C_{red1} + CO \rightleftharpoons C_{int} + CO_2 \quad (12)$$

$$C_{int} + CO \rightleftharpoons C_{red2} + CO_2 \quad (13)$$

Proton and hydroxide contributions to these equations were omitted because the pH of the solutions analyzed were fixed at either 6.3 or 8.0, and E^0_{CO/CO_2}(pH) appropriate for each pH were used. Equilibrium constants for reactions 2 and 5 will be called K_{tot} and K_{CO}, respectively. A_{red}-CO is probably generated from A_{ox} by a one-electron reduction and a CO-binding step, and this process was simulated assuming either reaction 2 or sequential reactions 3 and 5. The process was also modeled as requiring two electrons, reaction 4, and CO binding. The use of CO as a reductant in these reactions (and those involving the B-cluster) is not meant to imply that CO reduces A_{ox} or B_{ox} directly; only that equilibrium conditions with these clusters and the CO/CO_2 couple can be established. It is also known that B_{ox} is reduced by one electron, given by eq 6. However, the reduction was also modeled as requiring two electrons, indicated by eq 7. C_{red2} is probably two electrons more reduced than C_{red1}, but it is not known whether C_{red1} is reduced by CO directly to C_{red2}, as in eq 8, or if it is reduced first to the intermediate C_{int} state, and then to C_{red2}, as in eqs 9 and 10. Another model assumes that C_{red1} is reduced directly by four electrons to C_{red2}, eq 11, or by two electrons to the C_{int} state, and then by two more electrons to the C_{red2} state, eqs 12 and 13.

Equilibrium constants were converted to reduction potentials using the relation $K_i = \exp(nF/RT)\Delta E$, where n equals the number of electrons involved in the reaction, and $\Delta E = E^0_i(\text{pH}) - E^0_{CO/CO_2}(\text{pH})$. $E^0_{CO/CO_2}(6.3) = -0.487$ V and $E^0_{CO/CO_2}(8.0) = -0.587$ V (*31*). Equilibrium expressions, using molar concentrations of all species in solution and partial pressures for the two gases in these reactions, were solved at 100 simulation points (fixed partial pressures of CO (P_{CO}) and CO_2 (P_{CO_2})). Simulation of the titrations performed in an Ar atmosphere assumed a final $P_{CO_2} \sim 0.001$ atm,[4] estimated from a calculation of the amount of CO_2 generated as the system reached equilibrium using the Henry's law constant for CO_2, 3.1×10^3 μM/atm (*32*).

The quality-of-fit of the simulation to the data, Q_{fit}, was assessed as follows. For each of the N data points $P_{dat}(X_{dat}, Y_{dat})$, the normalized distance to every simulation point (X_{sim}, Y_{sim}) was determined according to eq 14

$$D_{sim} = \{[(X_{dat} - X_{sim})/(X_{max} - X_{min})]^2 + [(Y_{dat} - Y_{sim})/(Y_{max} - Y_{min})]^2\}^{1/2} \quad (14)$$

where ($X_{max} - X_{min}$) is the length of the data along the

[3] Menon and Ragsdale (*48*) recently reported that CODH solutions have a slow hydrogenase activity. This activity, if present in our samples, would have increased potentials by ~0.2 V relative to those calculated here. We measured the potential of CODH samples (1 mL of 1 mg/mL batch 3) under 1 atm CO_2 and various P_{CO} values (using an EG&G Princeton Applied Research Model 273 potentiostat, an electrochemical cell with a double-septum-sealed injection port, a Au working electrode, and a Ag/AgCl reference electrode). After injecting a known volume of CO, potentials of the stirred solution were monitored and then recorded after they stabilized, roughly 90 min after injecting CO. Additional CO was then injected and the process was repeated. Measured potentials were within 0.05 V of those calculated assuming no hydrogenase activity. Hydrogenase activity may be so slow in our samples as to have little effect on potentials, and so we have not taken it into account in our simulations.

[4] The minimum and maximum P_{CO_2} values present in these samples were estimated to be 0.0001 and 0.01 atm, respectively. The minimum corresponds to that generated by the oxidation of CO by CODH, while the maximum value is an estimate of possible residual amounts of CO_2 in the buffers (not eliminated during the degassing process), and that generated by the maximum amount of residual O_2 conceivably present. A 10-fold error in the estimate of P_{CO_2} translates into an error of ± 0.03 V.

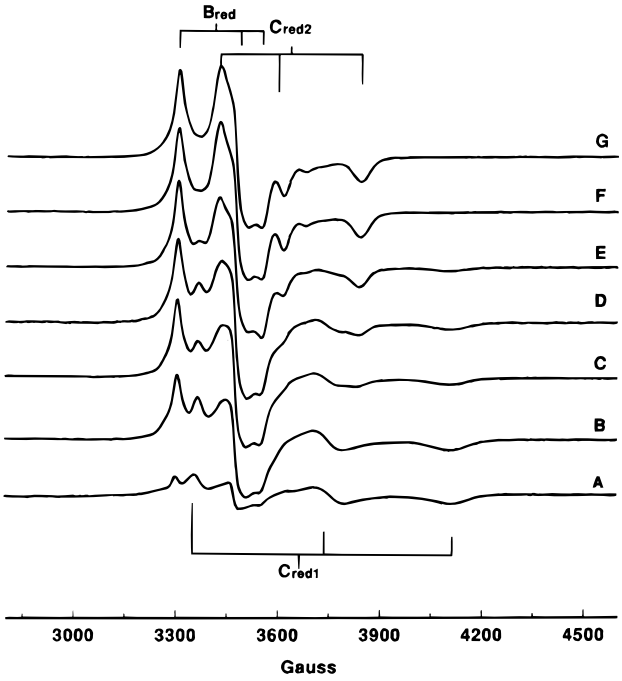

FIGURE 1: Selected EPR spectra of CODH poised at different partial pressures of CO under Ar at pH 8. Samples are from batch 1 as described in Experimental Procedures, and were poised at the following pCO: A, no CO; B, 4.24; C, 3.82; D, 3.46; E, 3.04; F, 2.69; G, 2.42. EPR conditions: microwave frequency, 9.43 GHz; temperature, 10 K; microwave power, 20 mW; modulation amplitude, 11.8 G; modulation frequency, 100 kHz. The *g* values of the $g_{av} = 1.94$, 1.82, and 1.86 signals, from the B_{red}, C_{red1}, and C_{red2} states, respectively, are indicated.

abscissa and $(Y_{max} - Y_{min})$ is the length of the data along the ordinate. The smallest D_{sim} value for each data point was designated D_{simmin}. For each titration, the quality-of-fit parameter, Q_{fit} was defined as

$$Q_{fit} = \frac{1}{N} \sum_{P_{dat}=1}^{N} D_{simmin} \qquad (15)$$

Each titration curve was simulated at different K_i values, and the lowest Q_{fit}, indicating the best-fit simulation, was designated Q_{bf}.

RESULTS

CO Titrations of CODH under Ar and CO_2 Atmospheres. Dithionite-free CODH samples were prepared at pH 8 in vessels containing increasing P_{CO} in a balance of Ar. Vessel volumes were sufficiently large so that the amount of CO reacting with the enzyme had a negligible effect on P_{CO}, and incubation times were sufficiently long for equilibrium to be established. Selected EPR spectra of these samples are shown in Figure 1. The sample poised at the lowest P_{CO} value exhibited the $g_{av} = 1.82$ and 1.94 signals, from the C_{red1} and B_{red} states, respectively. As P_{CO} increased, the $g_{av} = 1.82$ signal disappeared, and the $g_{av} = 1.86$, $g_{av} = 1.94$, and NiFeC signals developed.[5] These changes reflect the C_{red1}-to-C_{red2} conversion, the reduction of B_{ox} to B_{red}, and the reduction and CO-binding of A_{ox} to the A_{red}-CO state, respectively.

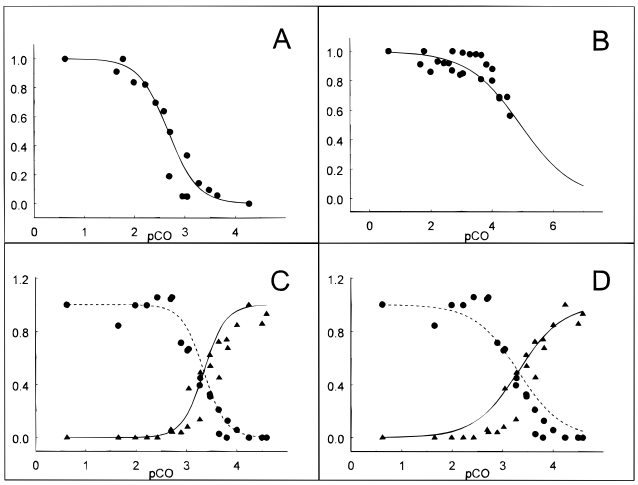

FIGURE 2: Normalized CODH EPR signal intensities vs pCO for titrations under Ar at pH 8. Points shown include the quantified intensities of the spectra in Figure 1 and the remaining spectra of the two sets of experiments performed. A, NiFeC signal (circles) and best-fit simulation using eq 2 with $K_{tot} = 1.0 \times 10^5$ atm^{-2} (solid line); B, $g_{av} = 1.94$ signal (circles) and best-fit simulation using eq 6 with $E^0_B(8.0) = -0.53$ V (solid line); C, $g_{av} = 1.82$ (triangles), $g_{av} = 1.86$ (circles), and best-fit simulation for C_{red1} and C_{red2} using eq 11 with $E^0_{C12}(8.0) = -0.58$ V (solid and dashed lines, respectively); D same as C except that the simulation was obtained using eq 8.

The individual signals contained in each spectrum (including those of Figure 1) were simulated and quantified. Normalized signal intensities are plotted vs P_{CO} in Figure 2. Plots of the NiFeC, $g_{av} = 1.94$, 1.82, and 1.86 signals will be called the A_{red}-CO, B_{red}, C_{red1}, and C_{red2} titration curves, respectively. At the lowest P_{CO} used, about half of the B-cluster population in the sample was already reduced, and so a full titration curve was not obtained. The potential at each point was estimated from P_{CO}, P_{CO_2}, the pH of the solution, and the Nernst equation. In the Ar titrations, P_{CO} and the pH were known, while P_{CO_2} was estimated to be 0.001 atm.[4]

Another group of samples was incubated in vessels containing 1 atm CO_2 and various fixed P_{CO}. Although the pH of the buffer used in these titrations was initially 8, the final pH of the solutions was ~6.3 after exposure to CO_2. Samples were frozen and analyzed by EPR (Figure 3). Plots of the normalized EPR signal intensities vs P_{CO} are shown in Figure 4. Relative to the titration performed under Ar, lower P_{CO} values were sufficient to yield fully developed signals in this titration. Moreover, the order of signal development was different; under CO_2, the B-cluster was reduced *after* the other states (i.e., at higher P_{CO} values than were needed to cause C_{red1} to decline and C_{red2} and A_{red}-CO to develop). Under Ar, the B-cluster was reduced at lower P_{CO} values. Since P_{CO_2} was known for these samples, accurate potentials could be calculated.

To determine whether these differences vis-à-vis the titrations performed under Ar were due to CO_2 or to the more acidic pH conditions employed in the CO_2 titration, a third experiment was performed in which samples were prepared in an Ar atmosphere at the pH of the CO_2 titration, namely pH = 6.3. Data were treated similarly, and the resulting

[5] NiFeC signals are not observed in Figure 1 because the A_{red}-CO state saturates at the microwave power employed. They were quantified under nonsaturating conditions (130 K, 80 mW).

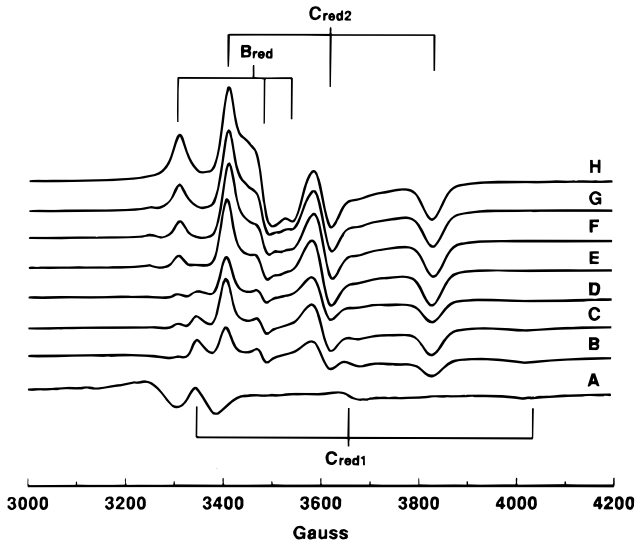

FIGURE 3: Selected EPR spectra of CODH poised at different partial pressures of CO under 1 atm CO_2. CODH (batch 2) poised at the following pCO values: A, no CO; B, 4.50; C, 4.18; D, 3.96; E, 3.65; F, 3.19; G, 2.69; H, 0. EPR conditions were the same as in Figure 1.

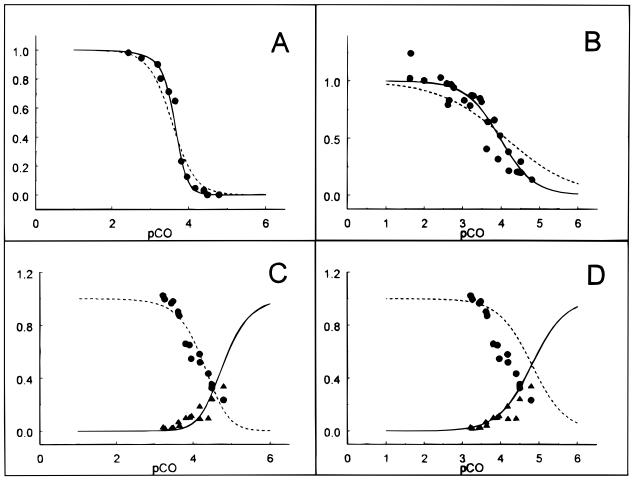

FIGURE 4: Normalized CODH EPR signal intensities vs pCO for the titrations under CO_2. Points shown include the quantified intensities of the spectra in Figure 3 and the remaining spectra of the two sets of experiments performed. A, NiFeC signal (circles), simulation using eqs 4 and 5, with $E^0_A = -0.39$ V, and $K_{CO} = 20000$ atm^{-1} (solid line), and simulation using eqs 3 and 5, with $E^0_A = -0.42$ V, and $K_{CO} = 23000$ atm^{-1} (dashed line); B, $g_{av} = 1.94$ signal (circles), simulation using eq 7 with $E^0_B(6.3) = -0.37$ V (solid), and simulation using eq 6 with $E^0_B(6.3) = -0.36$ V (dashed); C, $g_{av} = 1.82$ (triangles) and $g_{av} = 1.86$ (circles) signals, simulation of C_{red1} and C_{red2} using eqs 12 and 13, with $E^0_{C1N}(6.3) = -0.35$ V and $E^0_{CN2}(6.3) = -0.36$ V (solid and dashed lines, respectively); D, same as C except simulation using eq 8.

signal intensities are plotted vs P_{CO} in Figure 5. The order of the spectral changes that occurred as P_{CO} increased was the same as that observed under Ar at pH 8; development of B_{red} was followed by the C_{red1}-to-C_{red2} conversion and then by the rise of the A_{red}-CO state. Also, the P_{CO} values required to effect those changes were similar to those required for the Ar titration at pH 8, and were substantially greater than those required for the CO_2 titration. Although the pH had some effect on the curves, the presence of CO_2 appears to have caused the major difference between the first two titrations described.

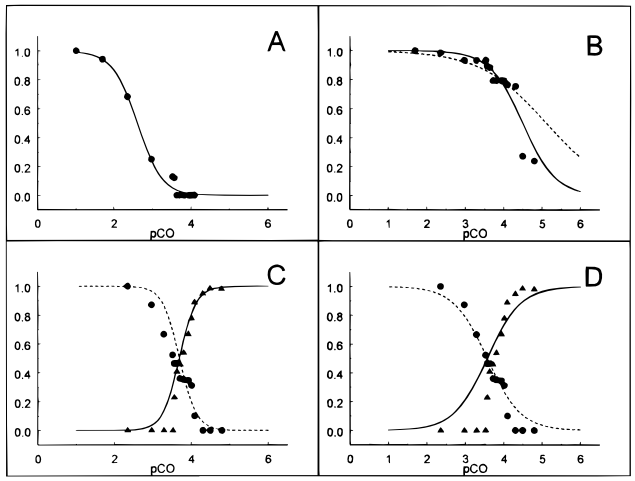

FIGURE 5: Normalized CODH EPR signal intensities vs pCO for the titration under Ar at pH 6.3. A, NiFeC signal (circles) and best-fit simulation using eqs 3 and 5, with $E^0_A = -0.52$ V and $K_{CO} = 1400$ atm^{-1} (solid line); B, $g_{av} = 1.94$ signal (circles), best-fit simulation using eq 7 with $E^0_B(6.3) = -0.46$ V (solid line), and best-fit simulation using eq 6 with $E^0_B(6.3) = -0.42$ V (dashed line); C, $g_{av} = 1.82$ (triangles), $g_{av} = 1.86$ (circles), and best-fit simulation for C_{red1} and C_{red2} using eq 11 with $E^0_{C12}(6.3) = -0.47$ V (solid and dashed lines, respectively); D same as C except that the simulation was obtained using eq 8.

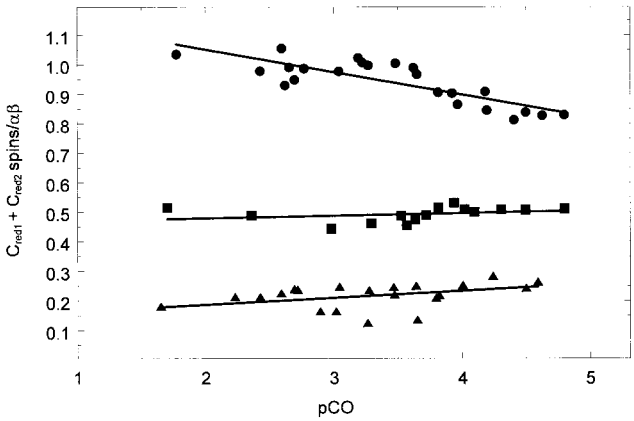

FIGURE 6: Summation of the $g_{av} = 1.82$ and 1.86 signal intensities from the three titrations plotted vs pCO. Circles, squares, and triangles represent the sums for the titrations performed under CO_2, Ar pH = 6.3, and Ar pH = 8.0, respectively. For clarity, squares and circles are displaced upward by 0.4 and 0.65 spins/$\alpha\beta$, respectively. Solid lines are linear best-fits, obtained using AXUM 3.0 (Trimetrix, Inc.).

For each of the three titrations, the sum of the $g_{av} = 1.82$ and 1.86 signal intensities were plotted as a function of P_{CO}. If the former signal converted directly into the latter, the sum of their intensities should be invariant throughout the titration. As shown in Figure 6, the plots for the titrations performed under Ar (squares and triangles) were essentially flat, while that performed under CO_2 (circles) had a noticeable slope with higher overall spin intensity from the C-cluster under higher P_{CO}. This suggests that at low P_{CO}, a significant proportion of C-clusters are in an EPR-silent state.

Effect of CO_2 on B_{red} Saturation/Relaxation Properties and CO/Acetyl-CoA Exchange Activity. In the course of analyzing these EPR spectra, we noticed that the $g_{av} = 1.94$ signal from B_{red} saturated substantially easier (lower microwave power at the same temperature) in the presence of CO_2 than

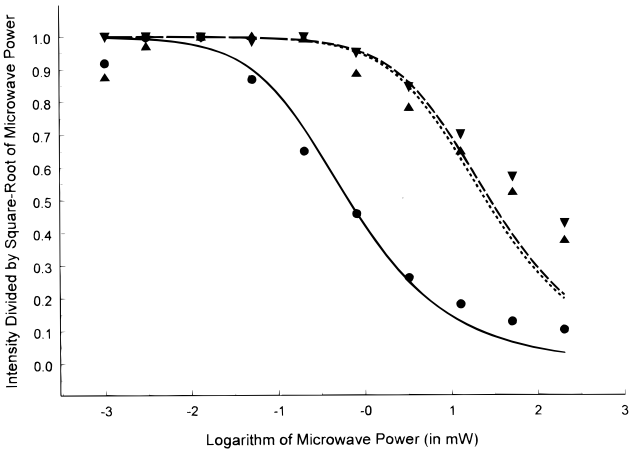

FIGURE 7: EPR 10 K power study of the $g_{av} = 1.94$ signal. Quantified signal intensities were divided by the square root of the microwave powers at which the spectra were obtained. These values were then normalized to the maximum value, and plotted vs the logarithm of the microwave power. Down-triangles, 4.3 mg/mL CODH in 50 mM Tris-Cl, pH 8.0, under $P_{Ar} = 0.84$ atm and $P_{CO} = 0.16$ atm. Up-triangles, 3.8 mg/mL CODH in 50 mM MES, pH 6.3, under $P_{Ar} = 0.83$ atm and $P_{CO} = 0.17$ atm. Circles, 4.3 mg/mL CODH in 50 mM Tris-Cl, pH 8.0 (final pH = 6.3), under $P_{CO_2} = 1$ atm and $P_{CO} = 1.6 \times 10^{-3}$ atm. The equation $S/\sqrt{P_{mw}} = P_{mw}/[(1 + P_{mw}/P_{1/2})]^{0.5B}$ (*49*) was fitted to the data. Fits were better when *B*, the inhomogeneity parameter, was set equal to 1. Dashed, dotted, and solid lines are best-fit curves using $B = 1$ and $P_{1/2}$ values of 9.2 mW (down-triangles), 8.2 mW (up-triangles), and 0.22 mW (circles), respectively.

in its absence. B_{red} signal intensities were divided by the square root of the microwave power, normalized to 1.0, and plotted vs. the log of the power in Figure 7. Such plots for the samples prepared under Ar at pH 8 and 6.3 indicate that the altered relaxation/saturation properties of the B_{red} cluster were due to the presence of CO_2, not to differences in pH.

We examined the effect of CO_2 on the CO/acetyl-CoA exchange activity of the enzyme. The exchange assay was performed using 20% CO in either an Ar or CO_2 atmosphere (both buffered at pH 6.3). The sample in Ar exhibited an activity of 0.55 units/mg, while that in CO_2 had only 0.02 units/mg activity. Two other samples were completely inhibited in CO_2 as well. We also determined that CO_2 did not inhibit the ability of 1,10-phenanthroline to remove the labile from the A-cluster.

Development of the NiFeC Signal in the Presence of Acetyl-CoA. Reduced CODH treated with 0.1 equiv/$\alpha\beta$ of acetyl-CoA exhibited a low-intensity NiFeC signal (Figure 8B). The intensity of this signal was 4% of that exhibited by a matching sample treated with 1 atm of CO (Figure 8A). Another sample treated with an excess of acetyl-CoA (3 equiv/$\alpha\beta$) did not exhibit a NiFeC signal (Figure 8C).

ANALYSIS

The A-Cluster. The A_{red}-CO state is obtained from A_{ox} by a reduction *and* a CO binding step, as shown in eqs 3 and 5. Consequently, the A_{red}-CO titration curves were simulated assuming these reactions and the input parameters E^0_A and K_{CO}. One problem with employing eqs 3 and 5 is that the A_{red} state, which ought to have an half-integer electronic spin and be EPR-active, has not been observed. The reason for this is unclear. One possibility is that CO-binding raises the reduction potential for the A_{ox}/A_{red} couple

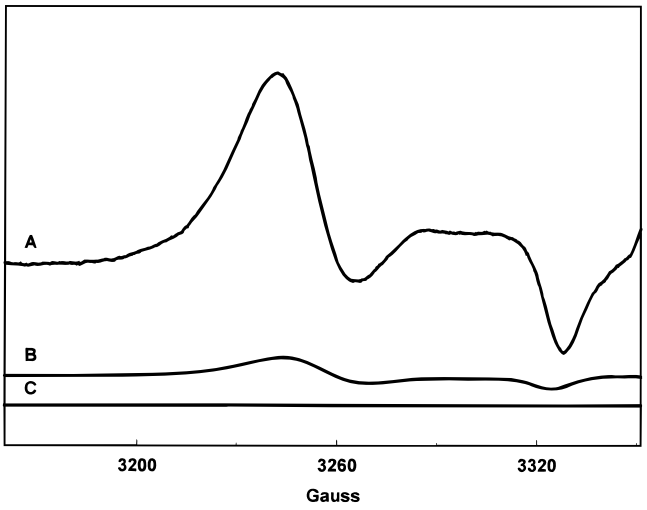

FIGURE 8: Background-subtracted EPR spectra of Ti(III)-citrate-reduced CODH in 0.1 (B), and 3 (C) equiv/$\alpha\beta$ of acetyl-CoA. A corresponding spectrum of Ti(III)-citrate-reduced CODH devoid of acetyl-CoA was used for subtractions. Spectrum A, a NiFeC signal quantifying to 0.21 spin/$\alpha\beta$, is from a matching CO-reduced sample. EPR conditions were as in the Figure 1 legend.

and that in the absence of CO the reductants typically employed are not sufficiently powerful to reduce A_{ox}.

When CO is the reductant, the uncertainty in how best to treat the absence of A_{red} can be avoided by fitting the data to eq 2. K_{tot} for eq 2 is related to K_{CO} and E^0_A by the relation shown in eq 16.

$$\ln K_{tot} = 2 \ln[K_{CO}] + [2F/RT](E^0_A - E^0_{CO/CO_2}(\mathrm{pH})) \quad (16)$$

This equation reveals why unique E^0_A and K_{CO} values cannot be obtained; namely, because a change in one can be counterbalanced by a change in the other to yield the same K_{tot}. Nevertheless, fitting A_{red}-CO titration curves using eqs 3 and 5 is fundamentally different from fitting them with eq 2.

In the former case, different combinations of E^0_A and K_{CO} (all yielding the same K_{tot}) will yield different proportions of enzyme in the A_{red} form throughout the simulated titration, while in the latter case A_{red} is undefined and always absent. Since A_{red} has not been observed, combinations of E^0_A and K_{CO} values yielding substantial proportions of A_{red} were excluded. High concentrations of A_{red} arise for combinations in which K_{CO} is relatively small and E^0_A is relatively large (i.e., when reducing A_{ox} is presumed to be thermodynamically "easy" and binding A_{red} "hard"), and such combinations will yield poorer-fitting simulations. Thus, we ignored combinations of E^0_A and K_{CO} on the extreme where substantial A_{red} was formed, namely when $Q_{fit} > 1.5Q_{bf}$. On the other extreme (when E^0_A is very negative and K_{CO} is very large), no such problem exists because essentially no A_{red} is formed. Thus, in principle, the magnitude of K_{CO} can increase without limit for a fixed K_{tot} because E^0_A can always be adjusted to more and more negative values. However, at some point K_{CO} becomes unrealistically large (and E^0_A unrealistically negative), and simulations past that point can be excluded. We have chosen the K_{CO} for the binding of CO to reduced myoglobin ($K_{CO} \sim 23000$ atm^{-1}; $K_d = 44$ nM) (*33*) as this limit.

Table 1: Best-Fit Parameters for the A_{red}-CO Titration Curves[a]

atm	pH	$[K_{CO}; E^0_A]_{min}$	$[K_{CO}; E^0_A]_{max}$	E^0_{NiFeC}	E^m_{NiFeC}
CO_2	6.3	6400; −0.39	23000; −0.42	−0.17	−0.38
Ar	6.3	430; −0.49	23000; −0.59	−0.35	−0.50
Ar	8.0	460; −0.59	23000; −0.69	−0.44	−0.60
Ar[b]	8.0	510; −0.58	23000; −0.68	−0.44	−0.60

[a] Simulated titration curves were fitted to the data as described in Experimental Procedures, using eq 2. Resulting best-fit K_{tot} values were converted to E^0_{NiFeC} by the relationship $RT \ln K_{tot} = nF(E^0_{NiFeC} - E^0_{CO/CO_2}(pH))$ where $E^0_{CO/CO_2}(6.3) = -0.487$ V and $E^0_{CO/CO_2}(8.0)$ −0.587 V. Curves generated using eqs 3 and 5 were fitted to the data as well, affording $[K_{CO}; E^0_A]$ pairs, each of which satisfy eq 19 when best-fit K_{tot} and appropriate $E^0_{CO/CO_2}(pH)$ values are employed. Maximum $[K_{CO}; E^0_A]$ values were obtained by fixing K_{CO} at 23000 atm^{-1} and determining the matching E^0_A. Minimum values were those at higher potential and weaker binding which generated a fit for which $Q_{fit} \sim 1.5Q_{bf}$. In a 2-dimensional graph in which K_{CO} and E^0_A are the axes, any point on the line segments connecting min and max values represents a $[K_{CO}; E^0_A]$ pair yielding an acceptable fit to the data. E^m_{NiFeC} values are the potentials at half-maximal NiFeC intensities. [b] Data from Shin and Lindahl (*16*).

Using these criteria, the best-fit values for fitting the A_{red}-CO titration curves are given in Table 1. The two titration curves performed under Ar yielded relatively similar K_{tot} values ($\sim 8 \times 10^4$ atm^{-1}) with no clear pH effect, while the value obtained for the titration under CO_2 (6×10^{10} atm^{-1}) was almost a million times greater. Best-fit $[E^0_A; K_{CO}]_{Ar}$ pairs (averaging results for both titrations) ranged from [−0.54 V; 450 atm^{-1}] to [−0.64 V; 23000 atm^{-1}]. These K_{CO} values correspond to $K_d = 44-3000$ nM. Best-fit $[E^0_A; K_{CO}]_{CO_2}$ pairs ranged from [−0.39 V; 6400 atm^{-1}] to [−0.42 V; 23000 atm^{-1}]. These K_{CO} values correspond to $K_d = 44-300$ nM. Thus, exposing the enzyme to CO_2 raises E^0_A by 0.12−0.25 V and possibly increases K_{CO} by as much as a factor of 60.

Before A_{red}-CO was realized to result from both reducing and binding CO to A_{ox}, Lindahl et al. (*6*) attempted to determined the redox potential associated with the development of this state by fitting a NiFeC titration curve using the Nernst equation and assuming the spurious half-cell reaction shown in eq 17.

$$A_{ox} + 1e^- \rightleftharpoons A_{red}\text{-CO} \qquad (17)$$

For samples poised electrochemically in a CO_2 atmosphere at pH 6.3, they obtained $E^m_{NiFeC} = -0.41 \pm 0.04$ V. Our data can be analyzed similarly, yielding $E^m_{NiFeC} = -0.38$ V. Comparable values for the other two titrations are given in Table 1 (yielding an average $E^m_{NiFeC} = -0.55$ V). However, such titrations must be analyzed using the correct half-cell reaction shown in eq 18.

$$A_{ox} + 1e^- + CO \rightleftharpoons A_{red}\text{-CO} \qquad (18)$$

The reduction potential for this couple, E^0_{NiFeC}, contains contributions of E^0_A and K_{CO},

$$E^0_{NiFeC} = E^0_A + [RT/F] \ln K_{CO} \qquad (19)$$

$E^0_{NiFeC} = -0.17$ V for our data obtained under 1 atm CO_2; other values are given in Table 1. Employing eq 17 in analyzing NiFeC titration curves is equivalent to assuming a particular (and fortuitously quite reasonable) value for K_{CO} (namely $K_d \sim 0.3$ μM for the CO_2 titration; 2 μM for Ar, pH 8).[6]

Gorst and Ragsdale (*15*) found that the NiFeC signal developed when CODH was electrochemically reduced in the presence of a molar excess of acetyl-CoA. They found that the NiFeC signal intensity increased as potentials were lowered, to about 10% of that obtained under 1 atm of CO. They fitted the resulting titration curve using the Nernst equation and calculated $E^m_{NiFeC} = -0.541$ V. We found that reduced CODH incubated in a substoichiometric amount of acetyl-CoA exhibited the NiFeC signal, but samples incubated in a molar excess of acetyl-CoA did not. We explain this by assuming that acetyl-CoA reacted quantitatively with reduced CODH to form the EPR-silent methyl-bound state (*34*), and that the freed CO reacted with the remaining nonmethylated CODH molecules, affording the observed low-intensity NiFeC signal. With a molar excess of acetyl-CoA, all CODH molecules appear to have been methylated and to be EPR-silent. We have more difficulty explaining the results of Gorst and Ragsdale (*15*) and are uncertain of the redox process to which their midpoint potential of −0.541 V corresponds.[7]

Shin and Lindahl (*16*) measured the development of the NiFeC signal in a stoichiometric CO titration of dithionite-reduced CODH, and simulated the resulting titration curve by iteratively solving CO-binding and reduction reactions using a procedure similar to that used here. They estimated

[6] The overall spurious redox reaction is $2A_{ox} + CO \rightleftharpoons 2A_{red}\text{-CO} + CO_2$, with half-cell couples $E = E^0_{CO/CO_2}(pH) - [RT/2F] \ln[P_{CO}/P_{CO_2}]$ and $E = E^m_{NiFeC} - [RT/F] \ln\{[A_{red}\text{-CO}]/[A_{ox}]\}$. E^m_{NiFeC} is the potential where the NiFeC signal reaches half-maximal intensity (i.e., when $[A_{red}\text{-CO}] = [A_{ox}]$), and $[P_{CO}]_{1/2}$ is the partial pressure of CO at that potential. For the 1 atm CO_2 data, $[P_{CO}]_{1/2} = 3.1 \times 10^{-4}$ atm. Equating two of the previous equations yields $E^m_{NiFeC} = E^0_{CO/CO_2}(6.3) - [RT/2F] \ln[P_{CO}]_{1/2} = -0.38$ V. Repeating this with the correct redox reaction ($2A_{ox} + 3CO \rightleftharpoons 2A_{red}\text{-CO} + CO_2$) and the correct half-cell reaction describing the development of the NiFeC signal, namely $E = E^0_{NiFeC} - [RT/F] \ln\{[A_{red}\text{-CO}]/([A_{ox}]P_{CO})\}$ yields the relationship (at half-maximal NiFeC intensity) $E^0_{NiFeC} = E^0_{CO/CO_2}(pH) - [RT/2F] \ln\{[P_{CO}]_{1/2}/[P_{CO_2}]_{1/2}\} - [RT/F] \ln[P_{CO}]_{1/2}$. Rewriting this in terms of E^m_{NiFeC} yields $E^0_{NiFeC} = E^m_{NiFeC} - [RT/F] \ln[P_{CO}]_{1/2} = -0.17$ V. Substituting eq 19 and generalizing to any pH yields $E^0_A + [RT/F] \ln K_{CO} = E^m_{NiFeC} - [RT/F] \ln[P_{CO}]_{1/2}$. $E^m_{NiFeC} = E^0_A$ when $K_{CO} = 1/[P_{CO}]_{1/2}$. Thus, the midpoint potential of the NiFeC titration curve equals E^0_A assuming a particular K_{CO}, namely $1/[P_{CO}]_{1/2}$.

[7] Our results and the mechanism proposed by Barondeau and Lindahl (*34*) both suggest that the NiFeC signal should not have been observed in their experiment. The extraneous signals and severe baseline drift evident in the spectrum illustrating their titration (see solid line, Figure 4, ref *15*) warrant concern that the signal assumed to be the NiFeC signal is not. However, if it is the NiFeC signal, it is reasonable to assume that a fraction of CODH reacted with acetyl-CoA to generate free CO, which bound (and possibly indirectly reduced) A-clusters in unreacted molecules. The results of our titration (Figure 2A) indicate that $P_{CO} \sim 5 \times 10^{-4}$ atm would yield a NiFeC signal with an intensity ~10% of maximal. Such a partial pressure could have been achieved, assuming a 5 mL gas-phase volume for their titrator and that ~1/3 of the 140 nmol of CODH present in solution reacted with acetyl-CoA to liberate CO. However, the variation of NiFeC signal intensity observed with changes in potential (yielding what appears to be a NiFeC titration curve) appears not to reflect a potential-dependent change in P_{CO}, like the curve shown in Figure 2A, since this curve does not plateau until $P_{CO} \sim 0.01$ atm. There was not enough CODH present in their experiment to produced partial pressures this high. The observed titration curve probably reflects another redox couple with a midpoint potential of −541 mV. Likely possibilities include the D_{ox}/D_{red}, A_{ox}/A_{red}, or CO_2/CO couples, but further studies are required to settle this issue.

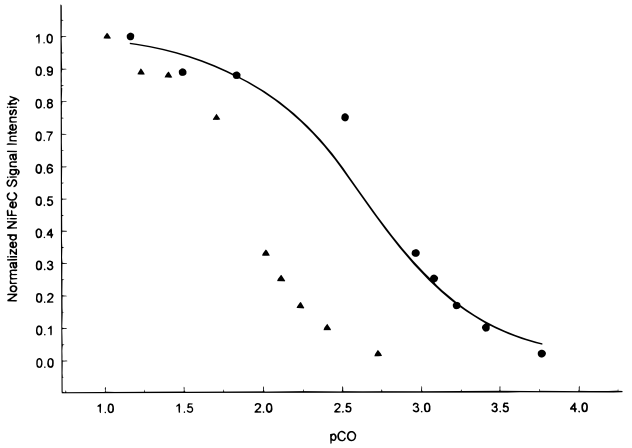

FIGURE 9: Reanalysis of the titration of Shin and Lindahl (*16*). Triangles, normalized NiFeC signal intensities vs initial pCO values. Circles, same data vs the calculated final pCO values. (Final pCO values differ from initial values because some CO was consumed during reaction with CODH.) Solid line, simulation assuming eqs 3 and 5 with $E^0_A = -0.65$ V and $K_{CO} = 8600$ atm^{-1}.

that $E^0_A = -0.54$ mV and $K_{CO} \sim 6-14$ atm^{-1},[2] corresponding to one possible solution with $K_{tot} \sim 4000$ atm^{-1}. This value of K_{tot} is substantially smaller than obtained here. To determine whether this discrepancy originated from the data or their analysis, we simulated their data (Figure 9) and obtained the best-fit parameters listed in Table 1. The similarity to the parameters obtained for our titrations suggests that the previous analysis underestimated K_{CO} for the value of E^0_A employed, but that their data is consistent with ours.[8]

The B-Cluster. B_{red} titration curves were analyzed using reaction 6 and the Nernst equation. Best-fit $E^0_B(8.0)$ values are given in Table 2. These potentials appeared pH-dependent, decreasing by ~ 0.06 V/pH unit. Adjusting the values obtained for the titration performed under Ar to pH 7 yields $[E^0_B(7.0)]_{Ar} = -0.47$ V. Lindahl et al. (*6*) reported an adjusted $[E^0_B(7.0)]_{Ar} = -0.43$ V, within error of that obtained here. Our best-fit $[E^0_B(7.0)]_{CO_2}$ value equals -0.41 V, ~ 0.06 V more positive than our $[E^0_B(7.0)]_{Ar}$.

Surprisingly, these titration curves generally fit better using Nernst equations with $n = 2$ (a two-electron process) than with $n = 1$, even though B_{red} is most certainly one electron more reduced than B_{ox}. For the titration under CO_2 and the Ar titration at pH 6.3, the best-fit simulation to eq 7 fit the data better by a factor of 2. The Ar titration at pH 8 (with more severe scatter) fit as well to simulations assuming either $n = 1$ or $n = 2$. Similarly, the A_{red}-CO titration curve obtained under CO_2 fit nearly 3 times better to an $n = 2$ reduction (eq 4) than to an $n = 1$ reduction (eq 3). There was no significant difference in the corresponding fits of the A_{red}-CO titration curves obtained under Ar.

The C-Cluster. Whether CO reduces C_{red1} directly to C_{red2}, as in eq 8, or whether the reduction proceeds through a one-electron intermediate state called C_{int}, as in eqs 9 and 10, is not known, and so the C_{red1} and C_{red2} titration curves were fitted to equations modeling both processes. Best-fit E^0_{C12}-(pH), E^0_{C1N}(pH), and E^0_{CN2}(pH) values and their associated Q_{fit} values are given in Table 3. For the titration in CO_2, the data fit nearly 2 times better to the model assuming the intermediate, with $[E^0_{C1N}(6.3)]_{CO_2} \sim [E^0_{CN2}(6.3)]_{CO_2}$. In contrast, the titrations in Ar fit better to the Direct-Conversion model (not proceeding through C_{int}). E^0_{C12}(pH) was pH-dependent, decreasing by 0.06 V/pH. $[E^0_{C12}(7.0)]_{CO_2}$ was -0.39 V while $[E^0_{C12}(7.0)]_{Ar}$ was -0.51 V (averaged values). Thus, the presence of a CO_2 atmosphere increased the reduction potential for the C_{red1}-to-C_{red2} conversion by 0.12 V. Lindahl et al. (*6*) previously measured $[E^0_{C12}(7.0)]_{CO_2}$ to be -0.40 V and $[E^0_{C12}(7.0)]_{Ar}$ to be -0.52 V (adjusting to pH = 7.0), similar to the values determined here.

All three sets of C_{red1} and C_{red2} titration curves fit better to simulations that assumed an overall $n = 4$ process, as specified in eqs 11−13, than to those assuming $n = 2$. Best-fit values are given in Table 3. The curve from the titration performed under CO_2 fit better to the Intermediate model, reactions 12 and 13, while those from the titrations performed under Ar fit better to the Direct Conversion model. The 67% increase in the sum of the C_{red1} and C_{red2} intensities as potentials are lowered suggests that about a third of the EPR-active C-clusters were in the C_{int} state at the lowest P_{CO} (highest potential) measured.

DISCUSSION

Reduction Potentials for CODH Redox Couples. A number of redox titrations of CODH have been reported, but an additional study was required because deficiencies in the earlier studies created a confusing and uncertain foundation upon which to base future investigations. Specifically, the $A_{ox} \rightarrow A_{red}$-CO reaction had been misanalyzed as a simple one-electron reduction, and even after the reaction was realized to involve both a reduction and a binding step, the inability to extract unique E^0_A and K_{CO} values from the NiFeC titration curve was not appreciated. A CO_2-induced shift in the redox potential associated with the development of the C_{red2} state was noted (*6*), but this effect was not satisfactorily characterized, as the titration was not performed under equilibrium conditions. Finally, no titrations using the substrates CO and CO_2 as redox agents had been reported. Since the enzyme operates in vivo in a CO_2 atmosphere, the redox properties under such circumstances may be especially relevant to catalysis.

The values obtained for E^0_B(pH) and E^0_{C12}(pH) for titrations performed in Ar and CO_2 atmospheres are within error of those obtained previously. This consistency provides evidence that these values are essentially correct and relatively free of systematic errors caused by different experimental setups. Our analysis reveals that unique values for E^0_A and K_{CO} cannot be obtained from NiFeC titration curves; rather only a range of acceptable pairs of values can be determined. Our reanalysis of previous studies generally provides a consistent view of the redox processes occurring in CODH.

CO binds to some Ni^{1+} tetrazamacrocyclic complexes with association constants K_{CO} as high as 10^2 atm^{-1} ($K_d \sim 10$ μM) (*35*). Carbon monoxide inhibits *Desulfovibrio gigas* hydrogenase by binding to the active site Ni with $K_i = 35$ μM ($K_{CO} \sim 30$ atm^{-1}) (*36*), and it binds to the oxidized iron-sulfur H-cluster of *Clostridium pasteurianum* (*37*) with $K_i = 1.1$ μM ($K_{CO} \sim 900$ atm^{-1}). Thus, the range of possible

[8] P. A. Lindahl and W. Shin retract their previous analysis and estimate of K_{CO} (*16*) which appear to have employed some spurious assumptions, but reaffirm the soundness of their data.

Table 2: Best-Fit Parameters for the B_{red} Titration Curves

atm	E^0_B(pH) $n = 1$	E^0_B (7.0) $n = 1$	E^0_B(pH) $n = 2$	E^0_B(7.0) $n = 2$	$Q_{bf}(n = 1)/Q_{bf}(n = 2)$
CO_2	−0.36 (pH = 6.3)	−0.41	−0.37 (pH = 6.3)	−0.41	2.0
Ar	−0.42 (pH = 6.3)	−0.46	−0.46 (pH = 6.3)	−0.50	2.0
Ar	−0.53 (pH = 8.0)	−0.47	−0.54 (pH = 8.0)	−0.48	1.1

Table 3: Best-Fit Parameters for the C_{red1}/C_{red2} Titration Curves

atm	$E^0_C = E^0_{C12} = E^0_{C1N} = E^0_{CN2}$ $n = 2$ and 4	E^0_C(7.0) $n = 2$ and 4	Q_{fit}(DC, $n = 2)/Q_{bf}$	Q_{fit}(DC, $n = 4)/Q_{bf}$	Q_{fit}(IN, $n = 2)/Q_{bf}$	Q_{fit}(IN, $n = 4)/Q_{bf}$
CO_2	−0.35 (pH = 6.3)	−0.39	1.7	1.3	1.2	**1.0**[a]
Ar	−0.47 (pH = 6.3)	−0.51	1.8	**1.0**[a]	2.9	1.4
Ar	−0.58 (pH = 8.0)	−0.52	1.6	**1.0**[a]	2.4	1.1

[a] Q_{fit} values for two models, one assuming Direct Conversion between C_{red1} and C_{red2} (called DC in the table) and the other assuming conversion through the C_{int} intermediate (called IN in the table) were compared. For each model, n values of 2 and 4 were evaluated for each of the three titrations listed in the rows of the table. Q_{fit} values for each simulation were normalized to Q_{bf}, the Q_{fit} resulting from the best-fit simulation. The resulting four Q_{fit}/Q_{bf} ratios for each titration are listed in their respective rows. The simulation yielding the best-fit for each titration is indicated by the Q_{fit}/Q_{bf} value **1.0** (indicated in bold).

K_{CO} values for binding to the A-cluster (K_d ranging from ~3 μM in Ar and 0.3 μM in CO_2 to 44 nM in either atmosphere) suggests that CO binds to the A-cluster as tightly, or more tightly, than it does to these related Ni and Fe centers. We favor the smaller K_{CO} values (weaker binding) because they are nearer to the K_{CO} values for these other systems, and the corresponding E^0_A values (~ −0.5 V) are closer to E^0_{CO/CO_2}(pH) and E^0 values for the other clusters in CODH. Thus, although we cannot strictly exclude stronger binding, we suspect that CO binds to the A-cluster with $K_d \sim 10^{-6}$ M in Ar and about an order-of-magnitude tighter in CO_2.

Redox Cooperativity. Cooperativity arises when one event affects subsequent similar events (*38*). Thus, redox cooperativity arises when the redox status of one site alters the reduction potential of another. Positive cooperativity arises when one center is reduced more easily once the other center is reduced, negative cooperativity arises when one center is thermodynamically more difficult to reduce when the other center is reduced, and noncooperativity arises when the redox status of one site has no effect on the reduction potential of the other. Titration curves of positively cooperating centers exhibit effective n values higher than those appropriate for the individual centers, while curves of negatively cooperating centers exhibit effective n values less than those appropriate for the individual centers.

It is virtually certain that the A- and B-clusters of CODH are reduced by one electron, yet the A_{red}-CO and B_{red} titration curves, at least for the titration performed in CO_2, fit better to simulations assuming an $n = 2$ process. Likewise, the reduction of C_{red1} to C_{red2} is most probably an $n = 2$ process, yet these titration curves fit better to $n = 4$ Nernst equations. These results indicate positive redox cooperativity in CODH, at least in the presence of CO_2, and possibly under Ar. Moreover, the coalescing of E^0_A, E^0_B(7.0), and E^0_{C12}(7.0) to within 20 mV of each other (−0.39 to −0.41, −0.41, and −0.39 V, respectively), when CO_2 is added to the enzyme, is remarkable. It means that, in the presence of CO_2, all three metal clusters in CODH undergo redox at essentially the same potential. These results suggest that in the presence of CO_2, CODH is reduced (in accordance with a midpoint potential of −0.40 V) by CO according to the following $n = 4$ process

$$[A_{ox}, B_{ox}, C_{red1}] + 3CO \rightleftharpoons [A_{red}\text{-}CO, B_{red}, C_{red2}] + 2CO_2$$

Redox cooperativity has been observed and analyzed in a number of multiple-redox-centered proteins, one of the most studied being the tetra-heme-containing cytochrome c_3 (*39*−*41*). Beef heart cytochrome oxidase appears to exhibit negative redox cooperativity, in that reducing one heme in the enzyme lowers the redox potential of the other heme by 0.135 V (*42*). The di-heme-containing cytochrome c_4 from *Pseudomonas stutzeri* also exhibits negative cooperativity, with $\Delta E^0 \sim 0.040$ V (*43*). The cooperativity in the latter protein was assumed to arise from electrostatic interactions between the two hemes, while that in the former was presumed to arise from a more complex mechanism (since the interacting hemes were known to be far apart).

NiFe hydrogenases contain a NiFe active site (stable in four sequential redox states called Ni-AB, Ni-SI, Ni-C, and Ni-R), two $[Fe_4S_4]^{2+/1+}$ clusters, and one $[Fe_3S_4]^{1+/0}$ cluster. Coremans et al. (*44*) found that in the absence of redox mediators, titration curves of the Ni-C/Ni-R transition, generated by reducing the enzyme with the substrate H_2, fit to $n = 2$ or $n = 4$ Nernst equations (depending on whether the quantified signal intensity was normalized to total Ni concentration or to EPR-active Ni) even though that transition is a one-electron process (Ni-C is $S = {}^1/_2$ while Ni-R is an even spin system). In contrast, in the presence of mediators, such curves fit to an $n = 1$ process. This unusually high n value is analogous to that observed for CODH, and it suggests positive redox cooperativity in NiFe hydrogenases.

The Effect of CO_2. Our study shows that the presence of CO_2 substantially alters the redox properties of the enzyme, specifically by increasing E^0_A, E^0_{C12}(pH), K_{CO}, possibly E^0_B-(pH), and by stabilizing the C_{int} state. We also demonstrated that CO_2 alters the relaxation/saturation properties of the $g_{av} = 1.94$ signal, and that, at least in the presence of CO_2, there is positive redox cooperativity. These changes may be related to other CO_2 effects observed previously. The presence of CO_2 has been found to shift the $g_{av} = 1.82$ signal (*10*), accelerate the dissociation of the inhibitor CN^- from the C-cluster in the presence of dithionite (*9*), and increase the rate at which dithionite converts C_{red1} to C_{red2}. Carbon dioxide also allows dithionite to reduce the A-cluster and to "cure" batches of CODH that had been unable to convert to

the C_{red2} state (*9*, *10*). Taken together, these results suggest that CO_2 binds to a site on the enzyme, and that this binding alters the environment, electron-transfer thermodynamics and kinetics, and ligand-binding properties of all the clusters in CODH. It would appear that CO_2 binding causes a major realignment of all three clusters and both subunits in CODH. We suspect that the CO_2 binding site effecting these changes is in the β-subunit, since some CO_2 effects (involving the dissociation of CN^-) are also known for the CODH from *Rhodospirillum rubrum* (*45*). This enzyme is a monomer with substantial genetic and spectroscopic homology to the β-subunit of the CODH from *C. thermoaceticum*. Carbon dioxide may interact at its substrate-binding site, presumed to be the Ni center of the C-cluster (*9*), or it may bind an "effector" site.

Given that acetyl-CoA is synthesized in-vivo in the presence of CO_2 (the bacteria are grown under a CO_2 atmosphere), one of the most fascinating results reported here is that CO_2 inhibits the CO/acetyl-CoA exchange activity of the enzyme. Both reactions presumably occur at the A-cluster and utilize the same mechanistic steps. Carbon dioxide is not a substrate for the A-cluster and 1,10-phenanthroline can remove the labile Ni of the A-cluster in the presence of CO_2, suggesting that CO_2 does not block access to the site. Our result that CO_2 strengthens the binding of CO to the A-cluster suggests that CO_2 inhibits exchange of bound CO. Together with other results presented here, it seems quite likely that CO_2-binding significantly alters the enzyme's mechanism of catalysis. The central importance of CO_2 in the physiology of acetogens adds to the potential importance of this CO_2-induced alteration.

The results presented here clarify the fundamental redox properties of the enzyme, and highlight the heretofore unnoticed importance of CO_2. They also provide direction for designing further experiments aimed at elucidating more details of the enzyme's unique bioorganometallic catalytic mechanism.

ACKNOWLEDGMENT

We thank Professor Woonsup Shin for helpful discussion.

REFERENCES

1. Ragsdale, S. W., and Kumar, M. (1996) *Chem. Rev. 96*, 2515−2539.
2. Halcrow, M. A., and Christou, G. (1994) *Chem. Rev. 94*, 2421−2481.
3. Xia, J., Sinclair, J. F., Baldwin, T. O., and Lindahl, P. A. (1996) *Biochemistry 35*, 1965−1971.
4. Anderson, M. E., DeRose, V. J., Hoffman, B. M., and Lindahl, P. A. (1993) *J. Am. Chem. Soc. 115*, 12204−12205.
5. Hu, Z., Spangler, N. J., Anderson, M. E., Xia, J., Ludden, P. W., Lindahl, P. A., and Münck, E. (1996) *J. Am. Chem. Soc. 118*, 830−845.
6. Lindahl, P. A., Münck, E., and Ragsdale, S. W. (1990) *J. Biol. Chem. 265*, 3873−3880.
7. Lindahl, P. A., Ragsdale, S. W., and Münck, E. (1990) *J. Biol. Chem. 265*, 3880−3888.
8. Kumar, M., Lu, W.-P., Liu, L., and Ragsdale, S. W. (1993) *J. Am. Chem. Soc. 115*, 11646−11647.
9. Anderson, M. E., and Lindahl, P. A. (1994) *Biochemistry 33*, 8702−8711.
10. Anderson, M. E., and Lindahl, P. A. (1996) *Biochemistry 35*, 8371−8380.
11. Seravalli, J., Kumar, M., Lu, W.-P., and Ragsdale, S. W. (1995) *Biochemistry 34*, 7879−7888.
12. Fan, C., Gorst, C. M., Ragsdale, S. W., and Hoffman, B. M. (1991) *Biochemistry 30*, 431−435.
13. Xia, J., Hu, Z., Popescu, C. V., Lindahl, P. A., and Münck, E. (1997) *J. Am. Chem. Soc. 119*, 8301−8312.
14. Xia, J., and Lindahl, P. A. (1996) *J. Am. Chem. Soc. 118*, 483−484.
15. Gorst, C. M., and Ragsdale, S. W. (1991) *J. Biol. Chem. 266*, 20687−20693.
16. Shin, W., and Lindahl, P. A. (1992) *Biochemistry 31*, 12870−12875.
17. Shin, W., and Lindahl, P. A. (1992) *J. Am. Chem. Soc. 114*, 9718−9719.
18. Ragsdale, S. W., Ljungdahl, L. G., and DerVartanian, D. V (1982) *Biochem. Biophys. Res. Commun. 108*, 658−663.
19. Ragsdale, S. W., Wood, H. G., and Antholine, W. E. (1985) *Proc. Natl. Acad. Sci. U.S.A. 82*, 6811−6814.
20. Kumar, M., Lu, W.-P., Liu, L., and Ragsdale, S. W. (1994) *Biochemistry 33*, 9769−9777.
21. Shin, W., and Lindahl, P. A. (1993) *Biochim. Biophys. Acta 1161*, 317−322.
22. Pelley, J. W., Garner, C. W., and Little, G. H. (1978) *Anal. Biochem. 86*, 341−343.
23. Morton, T. A., Rundquist, A. R., Ragsdale, S. W., Shanmugasundaram, T., Wood, H. G., Ljungdahl, L. G. (1991) *J. Biol. Chem. 266*, 23824−23828.
24. Raybuck, S. A., Bastian, N. R., Orme-Johnson, W. H., and Walsh, C. T. (1988) *Biochemistry 27*, 2698−2702.
25. Zehnder, A. J. B., and Wuhrmann, K. (1976) *Science 194*, 1165−1166.
26. Belford, R. L., and Nilges, M. J. (1979) *Computer Simulation of Powder Spectra EPR Symposium, 21st Rocky Mountain Conference, August*, 1979, *Denver*.
27. Nilges, M. J. (1981) *Electron Paramagnetic Resonance Studies of Low Symmetry Nickel I and Molybdenum V Complexes*, Ph.D. Dissertation, University of Illinois at Urbana-Champaign.
28. Altman, T. E. (1981) *Analysis of Nuclear Quadrupole Coupling in EPR Spectra*, Ph.D. Dissertation, University of Illinois at Urbana-Champaign.
29. Dubila, E. P. (1983) *Studies of Nuclear Quadrupole Effects in Transition Metal Complexes by Electron Paramagnetic Resonance*, Ph.D. Dissertation, University of Illinois at Urbana-Champaign.
30. Orme-Johnson, N. R., and Orme-Johnson, W. H. (1978) *Methods Enzymol. 52*, 252−257.
31. Reiger, P. H. (1994) *Electrochemistry*, Chapman & Hall, New York.
32. Butler, J. N. (1982) *Carbon Dioxide Equilibria and Their Applications*, Addison-Wesley, Reading, MA.
33. Collman, J. P., Halbert, T. R., and Suslick, K. S. in *Metal Ion Activation of Dioxygen* (Spiro, T., Ed.) (1980) pp 1−72, J. Wiley, New York.
34. Barondeau, D. P., and Lindahl, P. A. (1997) *J. Am. Chem. Soc. 119*, 3959−3970.
35. Gagné, R. R., and Ingle, D. M. (1981) *Inorg. Chem. 20*, 420−425.
36. Fauque, G., Peck, H. D., Jr., Moura, J. J. G., Huynh, B. H., Berlier, Y., Der Vartanian, D. V., Teixeira, M., Przybyla, A. E., Lespinat, P. A., Moura, I., and LeGall, J. (1988) *FEMS Microbiol. Rev. 54*, 299−344.
37. Adams, M. W. W. (1987) *J. Biol. Chem. 262*, 15054−15061.
38. Neet, K. E. (1995) in *Methods Enzymol. 249*, 519−567.
39. Santos, H., Moura, J. J. G., Moura, I., LeGall, J., and Xavier, A. V. (1984) *Eur. J. Biochem. 141*, 283−296.
40. Coletta, M., Catarino, T., LeGall, J., and Xavier, A. V. (1991) *Eur. J. Biochem. 202*, 1101−1106.
41. Turner, D. L., Salgueiro, C. A., Catarino, T., LeGall, J., and Xavier, A. V. (1996) *Eur. J. Biochem. 241*, 723−731.
42. Babcock, G. T., Vickery, L. E., and Palmer, G. (1978) *J. Biol. Chem. 253*, 2400−2411.

43. Conrad, L. S., Karlsson, J. J., and Ulstrup, J. (1995) *Eur. J. Biochem. 231*, 133−141.
44. Coremans, J. M. C. C., van Garderen, C. J., and Albracht, S. P. J. (1992) *Biochim. Biophys. Acta 1119*, 148−156.
45. Hyman, M. R., Ensign, S. A., Arp, D. J., and Ludden, P. W. (1989) *Biochemistry 28*, 6821−6826.
46. Wilhelm, I., Battino, R., and Wilcock, R. J. (1977) *Chem. Rev. 77*, 219−262.
47. Budavari, S., Ed. (1989) in *The Merck Index*, 11th ed., Merck & Co., Rahway, NJ.
48. Menon, S., and Ragsdale, S. W. (1996) *Biochemistry 35*, 15814−15821.
49. Rupp, H., Rao, K. K., Hall, D. O., and Cammack, R. (1978) *Biochim. Biophys. Acta 537*, 255−269.

BI980149B